



Silicon nitride membrane mirrors for focus control
by Robert Andreas Friholm

A thesis submitted in partial fulfillment of the requirements for the degree of Masters of Science in
Electrical Engineering
Montana State University
© Copyright by Robert Andreas Friholm (2001)

Abstract:

This thesis is an investigation into the feasibility of using deformable silicon nitride membrane mirrors for focus control without introducing spherical aberrations. The mirrors are circular with sizes ranging from 300 μ m to 1500 μ m diameter. Focus control is achieved by deflecting the membranes, while maintaining a parabolic surface shape, as not to introduce spherical aberrations. The deflection of the membranes is done electrostatically and uses two concentric actuation zones for spherical aberration control. Variation in the membrane boundary conditions was investigated to determine the effect on spherical aberration in the mirrors. The devices were built using a method which is a hybrid between surface and bulk micromachining. The fabrication method enables the air gap beneath the membrane to be precisely controlled to the desired depth. Devices 1500 μ m in diameter displayed focal length adjustments ranging from infinity to 39mm, corresponding to membrane displacement of 3.6 μ m at membrane center.

It was shown that spherical-aberration-free focus control was possible to achieve using the two-actuation-zone configuration. The devices were found to have resonant frequencies in the 20-25kHz range, which makes the devices suitable for real time video rate focus control. Integration of a device into a confocal microscope with object space numerical aperture yielded a change in focal plane location of 75 μ m, with insignificant impact on system performance. It was therefore concluded that the devices are suitable for spherical aberration free focus control at relatively high frequencies.

SILICON NITRIDE MEMBRANE MIRRORS FOR FOCUS CONTROL

By

Robert Andreas Friholm

A thesis submitted in partial fulfillment
of the requirements for the degree

of

Masters of Science

in

Electrical Engineering

MONTANA STATE UNIVERSITY
Bozeman, Montana

August 2001

N378
F9164

APPROVAL

of a thesis submitted by

Robert Andreas Friholm

This thesis has been read by each member of the thesis committee and has been found to be satisfactory regarding content, English usage, format, citations, bibliographic style, and consistency, and is ready for submission to the College of Graduate Studies.

David Dickensheets
Committee Chair

David H. Dickensheets
(Signature)

Aug 14, 2001
(Date)

Approved for the Department of Electrical & Computer Engineering

Jim Peterson
Department Head

James N. Peterson
(Signature)

8/21/01
(Date)

Approved for the College of Graduate Studies

Bruce M^cLeod
Graduate Dean

Bruce M^cLeod
(Signature)

8-24-01
(Date)

STATEMENT OF PERMISSION OF USE

In presenting this thesis in partial fulfillment of the requirements for a master's degree at Montana State University, I agree that the Library shall make it available to borrowers under the rules of the Library.

If I have indicated my intention to copyright this thesis by including a copyright notice page, copying is allowable only for scholarly purposes, consistent with "fair use" as prescribed in the U.S. Copyright Law. Requests for permission for extended quotation from or reproduction of this thesis in whole or in parts may be granted only by the copyright holder.

Signature

Robert Fréholm

Date

8/15/01

TABLE OF CONTENTS

1. INTRODUCTION	1
2. THEORETICAL DEVELOPMENT	5
Target Specifications	5
Parabolic Mirror	5
Mechanical Behavior	10
Membrane Actuation	11
Modeling	12
3. DESIGN.....	16
Material / Structural Choices / Fabrication Constraints.....	16
Proposed Device	17
Boundary Conditions	18
Actuation Regions.....	19
Etch Holes.....	20
Secondary Concerns.....	21
Final Device Idea	22
4. MAKING THE DEVICES	23
Process Flow	23
Considerations.....	26
Layout	27
Release Process.....	30
Considerations.....	31
Imaging of Release Process	34
Results ³ Oxide Etch.....	35
Results Silicon Etch.....	39
Summary	42
Recommendations.....	43
5. RESULTING DEVICES	44
Optical Profilometer.....	44
Profilometer Setup	45
Profilometer Measurement / Post-processing	46
Optical Profilometer Results.....	47
Dynamic Measurements.....	53
Device Issues	58

TABLE OF CONTENTS - CONTINUED

6. INTEGRATION INTO MARS PROBE.....	60
Mars Probe Setup.....	60
Benchtop Integration.....	61
Miniature Probe Integration.....	64
Theoretical Treatment.....	64
Integration.....	67
Summary.....	69
7. CONCLUSIONS.....	72
BIBLIOGRAPHY.....	75

LIST OF TABLES

Table	Page
2-1. Results from FEA simulations on 1500 μm device with segmented and thinned support.....	15
5-1. Obtained f_0 and Q values of various devices from curve fits of dynamic response data from device with 12 μm pit depth.....	57

LIST OF FIGURES

Figure	Page
2-1. Imaging of a collimated beam by a a) Spherical reflector b) Parabolic reflector.....	6
2-2. Incident collimated beam on spherical reflector and thin lens a) Collimated beam is imaged at focal point of spherical reflector b) Collimated beam is imaged at focal point of thin lens.....	7
2-3. Radius of spherical reflector as function of device radius and deflection.....	8
2-4. Resulting focal length of 750 μ m and 1500 μ m diameter device from deflection at center of device	9
2-5. Finite element model of membrane structure	13
2-6. FEA simulation results from actuation of 1500 μ m device by pressure on inner, outer, and both actuation zones	15
3-1. Conceptual cross-sections of polysilicon device (surface micro- machining) and silicon nitride device (hybrid between surface and bulk micromachining)	17
3-2. Design layout of a 300 μ m diameter device with 10% duty width and weakened edge support	19
4-1. Fabrication sequence for the membrane mirrors	25
4-2. Mask layers of the membrane mirrors	28
4-3. SEM picture of 1500 μ m device with segmented but no thinning of the edge support	29
4-4. SEM images of membrane devices illustrating key features a) Lateral etch-stop and thinned support of circular device b) Metal trace crossing back-filled etch stop trench c) Close-up of thinned edge support d) Segmented thinned support of broken square device	30

LIST OF FIGURES - CONTINUED

Figure	Page
4-5. Setup for imaging of silicon etching process	35
4-6. SEM image of broken device, illustrating where devices with thinned edge support break	36
4-7. Crack in membrane structure terminating in etch hole	36
4-8. Wave propagating across 1000 μ m 10% device as pillars beneath membrane are etched away a) Wave propagates from perimeter of device b) Wave reaches center actuation zone c) Amount of remaining pillars is less than diameter of center actuator d) Device is freestanding	38
4-9. Frames from video of TMAH silicon etch (up is to the left) a) Steady stream of bubbles coming out of a few vias b) Stream of bubbles cease c) Large bubble is forming beneath membrane d) Explosive burst, releasing hydrogen bubbles	40
4-10. SEM images illustrating bottom profile of different devices a) Bottom of pit beneath device with segmented support b) Device with continuous support	42
5-1. 1500 μ m 10% membrane with no thinning of edge support a) Perfectly flat die with 200v applied to both actuation zones b) Tilted membrane (to give straight lines across it), 0v applied c) Tilted membrane, 200v applied to both actuation zones	45
5-2. Optical profilometer setup using a Mireu interferometer objective lens	46
5-3. Deflection vs. Applied Voltage graph of a 1500 μ m device with 10% duty width, no thinning of the edge support, and 12 μ m pit depth	48
5-4. Surface profile data and curve fit of 1500 μ m 10% device without thinned edge support, with 0v and 200v applied on both actuation zones	50

LIST OF FIGURES - CONTINUED

Figure	Page
5-5. Images of 1500 μ m 10% device with no thinning of edge support a) Actuation voltages: 150v on inner actuation zone, 0v on outer b) Actuation voltages: 0v on inner actuation zone, 150v on outer c) Actuation voltages: 150v on both actuation zones	51
5-6. Surface profile data and curve fit of 1500 μ m 10% device without thinned edge support, with 150v applied to inner, outer, and both actuation zones.....	51
5-7. Actuation voltage pairs where spherical aberration goes through zero point.....	53
5-8. Data from dynamic response measurement and low pass curve fit of 1500 μ m 10% device. curve fit gave $f_0 = 19.3\text{kHz}$ and $q = 0.4977$	54
5-9. Data from dynamic response measurement and low pass curve fit of 1500 μ m 100% device. curve fit gave $f_0 = 22.3\text{kHz}$ and $q = 0.503$	55
5-10. Data from dynamic response measurement and low pass curve fit of 300 μ m 10% device. curve fit gave $f_0 = 25.9\text{kHz}$ and $q = 0.564$	55
5-11. Second order low pass curve fit to dynamic response measurements of 1500 μ m 10%, 1500 μ m 100%, and 300 μ m 10% devices without thinning of support.....	56
5-12. Graph of leakage current as function of applied voltage on a bonding pad (which is not connected to a device)	58
6-1. Optical setup of benchtop CMarS integration	61
6-2. Images obtained at focusing extremes of 750 μ m membrane a) 0v applied to membrane (no deflection) b) 200v applied to membrane (1.2 μ m deflection).....	63
6-3. Miniature system with membrane mount integrated	64

LIST OF FIGURES - CONTINUED

6-4. Lens configuration of miniature probe	65
6-5. Focus control of miniature system as a function of center deflection of incorporated 1500 μ m device (paraxial case).....	66
6-6. Membrane mount for integration into CMaRS probe	
a) Mount with small die containing two 1500 μ m devices	
b) Wire-bonds from 0 Ω resistors to bonding pads of 1500 μ m 10% device	67

ABSTRACT

This thesis is an investigation into the feasibility of using deformable silicon nitride membrane mirrors for focus control without introducing spherical aberrations. The mirrors are circular with sizes ranging from 300 μm to 1500 μm diameter. Focus control is achieved by deflecting the membranes, while maintaining a parabolic surface shape, as not to introduce spherical aberrations. The deflection of the membranes is done electrostatically and uses two concentric actuation zones for spherical aberration control. Variation in the membrane boundary conditions was investigated to determine the effect on spherical aberration in the mirrors. The devices were built using a method which is a hybrid between surface and bulk micromachining. The fabrication method enables the air gap beneath the membrane to be precisely controlled to the desired depth. Devices 1500 μm in diameter displayed focal length adjustments ranging from infinity to 39mm, corresponding to membrane displacement of 3.6 μm at membrane center. It was shown that spherical-aberration-free focus control was possible to achieve using the two-actuation-zone configuration. The devices were found to have resonant frequencies in the 20-25kHz range, which makes the devices suitable for real time video rate focus control. Integration of a device into a confocal microscope with object space numerical aperture yielded a change in focal plane location of 75 μm , with insignificant impact on system performance. It was therefore concluded that the devices are suitable for spherical aberration free focus control at relatively high frequencies.

CHAPTER 1

INTRODUCTION

The first Microelectromechanical system (MEMS) device was made in the mid-1960s, when a resonating MOS gate structure was built at Westinghouse [1]. It was not until the late 1980s that the field of MEMS started gaining ground and the term MEMS, itself, was not officially adopted until 1989 [2]. Since then, significant advancements have been made in the area. The main reason for the fast development of the technology is that MEMS uses existing CMOS technology that has evolved over the last decades with the rapid development of the microprocessor and memory industry [3]. As the minimum feature size of MEMS structures normally is around a few microns, older CMOS equipment can be used, which lowers production cost. Since MEMS devices can be produced by batch processing, large volumes can be produced at low cost per individual device.

Silicon has very good material properties (comparable to steel) and very durable and versatile structures can be constructed from it. MEMS processes are CMOS compatible, which makes it possible to create a monolithic integration with mechanical and microelectronic parts on the same chip and reduce the part size of the system.

The ability to create mechanical structures with or without integrated electronics on a small scale using silicon wafers has vast benefits in several applications. The automotive industry, which has been the driving force behind the sensor technology of

MEMS, uses MEMS accelerometers to control deployment of airbags. Because of the small size and relatively low cost of the devices redundant sensors can be installed for increased reliability with low overhead.

The information technology industry is another major contributor to the growth of MOEMS technology (Micro-opto-electromechanical systems). As fiberoptic communication has grown with the expansion of the internet, small and reliable MOEMS devices can be used in applications such as fiberoptic switches to reroute incoming optical signals to any of a number of outgoing fibers.

Considerable attention has been dedicated to the development of adaptive optics using MOEMS technology. The bulk of the adaptive optics is focused on correcting for random aberrations in applications such as ground based telescopes used in astronomy, where Earth's atmosphere introduces random aberrations [4, 5]. These are complex devices with large grids of actuators that control the surface shape of the mirrors. Some devices are focused on correcting for one specific type of aberration and can therefore use simple mirror shapes that are already known. These devices generally correct for one of the primary (Seidel) aberrations of a system such as defocus [6, 7, 8, 9], spherical aberration, and astigmatism [10]. Using compensating adaptive optics, correcting for known aberrations, will enable cheaper lenses of lower optical quality to be utilized in optical systems at a lower cost, but with performance comparable to more expensive systems.

In this thesis, deformable mirrors for focus control are presented. Previous efforts toward focus control have been made based on a number of different concepts. Burns and Bright [7] designed a thermally controlled focusing mirror capable of frequencies beyond 120Hz with a maximum power consumption of 480mW. Concentric rings of aluminum on the polysilicon membrane surface acts as a reflector and the largest ring, when resistively heated, causes the membrane curvature to change due to the change in residual stress of the materials. Zhu and Sun [6] demonstrated aberration free focusing using a 19-channel deformable silicon nitride membrane mirror with a diameter of 1cm. The bottom of the membrane structure has 19 independent hexagonal actuation zones, which causes the aluminum-coated membrane to deflect due to electrostatic force caused by the applied voltages. A lookup table is used to control the voltages of the actuators below the mirror to maintain aberration free imaging at frequencies ranging up to hundreds of Hertz. Vdovin and Sarro [8] produced mirrors with a clear aperture of 1cm, capable of focal lengths ranging from ∞ (flat mirror) to 0.25m at frequencies up to 75Hz. A 19-channel actuation scheme similar to the one used by Zhu and Sun is employed by these deformable membrane mirrors. Derivations of these mirrors are now commercially available in sizes ranging from 5mm to 50mm, actuation schemes with 19 to 119 channels, and frequency responses of up to 500Hz.

Our devices are circular, low stress, silicon nitride membrane structures on the order of a millimeter in diameter that are suspended across a pit in the bulk silicon beneath it. They operate on the principle that a mirror with a cross sectional parabolic surface figure acts as a positive lens. By deflecting the mirror to varying degrees, the

level of curvature of the mirror changes, which moves the location of the focal point of the mirror. Two topside gold electrodes electrostatically control the amount of deflection of the mirrors and also make up the reflective surface of the mirrors. By adjusting the control voltages of the two independent actuation zones, the membranes can maintain zero spherical aberration. The target voltage range for surface control of the mirrors is below 200V for a deflection of a few microns, which yields a focal length range from ∞ to 0.04m. The devices have frequency responses in the 20-25kHz range, which makes them suitable for real time video rate focus control.

The mirrors are intended for integration into a confocal microscope and Raman spectrometer (CMaRS) probe that uses beam scanning to compose an image [11]. The probe will be attached to a robotic arm in a rover-based vehicle for Mars exploration. The robotic arm is used for moving the probe up to the sample. The final adjustment of the focal plane is performed by the adaptive optics of the probe, which enables the probe to image samples that are not perfectly flat by adjusting for optimal focus across the field of view of the sample. At this point the focus control of the probe is done by a lens-mount which is moved by a piezoelectric actuator. Integration of a deformable mirror would decrease the overall weight and size of the system and the low power consumption of an electrostatically controlled membrane mirror is ideal for applications with limited available power.

CHAPTER 2

THEORETICAL DEVELOPMENT

Target Specifications

A membrane device with a reflective surface with good optical quality is desired. In order to maintain spherical aberration free imaging, it needs to maintain a perfectly parabolic shape when deflected. Means of controlling the surface shape of the membrane to maintain a parabolic shape need to be implemented, as the device is expected to deviate from a perfectly paraboloidal shape under uniform pressure. The device is desired to be able to achieve a large enough deflection to give 200 μm of focus control for a given system (discussed in chapter 6). The voltage required to achieve this actuation should ideally be less than 200V to avoid electric breakdown of the device.

Parabolic Mirror

In order to maintain an aberration-free imaging system with a membrane device, the surface shape of the membrane needs to be parabolic (assuming collimated incident illumination). This is illustrated in figure 2-1, where a spherical reflector and a parabolic reflector are shown together. In a) it is noted that the rays of a collimated beam do not come to a perfect focus, but are in fact spread around the focal point by the spherical mirror. This is known as spherical aberration. The incoming rays from the collimated

beam are reflected by the parabolic mirror in b) and come to a perfect focus at the focal point, f .

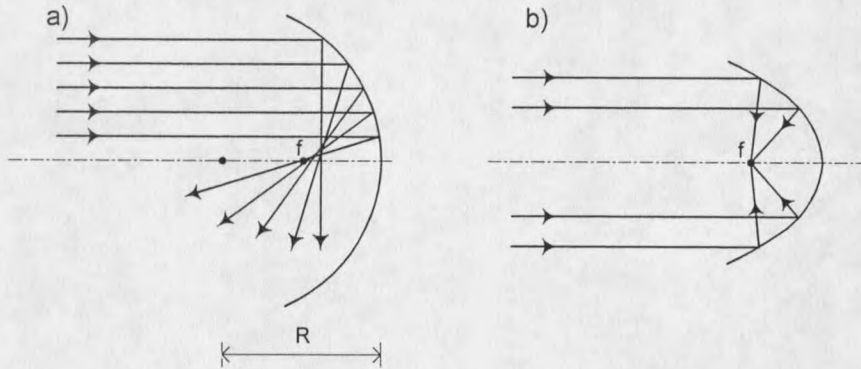


Figure 2-1. Imaging of a collimated beam by a
 a) Spherical reflector
 b) Parabolic reflector

For the paraxial case (rays close to the optical axis), a spherical reflector acts like a paraboloidal mirror of focal length $f = R/2$ (R is the radius of the spherical mirror). Figure 2-2 shows the concept of how a reflective spherical surface acts as a positive lens. The governing equation for imaging with a spherical mirror is

$$\frac{1}{z_1} + \frac{1}{z_2} = -\frac{2}{R}, \quad (2-1)$$

where z_1 is the distance from the mirror to the object, z_2 is the distance from the mirror to the image, and R is the radius of the mirror. The conventions of the formula are as shown in figure 2-2 a). The minus sign of the radius denotes a concave mirror. For a thin lens, the corresponding equation is

$$\frac{1}{z_1} + \frac{1}{z_2} = \frac{1}{f}, \quad (2-2)$$

where z_1 is the distance from the lens to the object, z_2 is the distance from the lens to the image, and f is the focal length of the lens. The conventions of the formula are as displayed in figure 2-2 b).

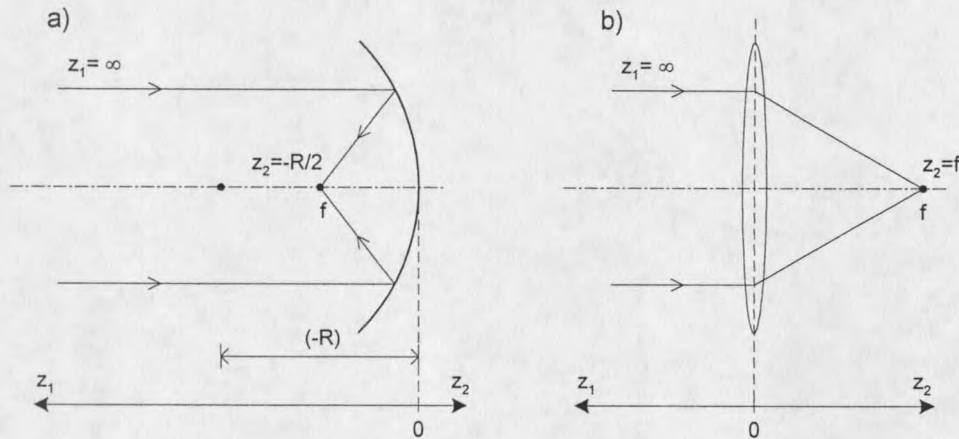


Figure 2-2. Incident collimated beam on spherical reflector and thin lens.

- a) Collimated beam is imaged at focal point of spherical reflector.
- b) Collimated beam is imaged at focal point of thin lens.

Since z_1 is at infinity for the two cases shown above, the location of the image is found to be at $R/2$ for the spherical mirror, and at f for the thin lens. The radius of (2-1) depends on the radius and the amount of deflection of the device. Figure 2-3 shows how the radius of the spherical mirror was derived from the deflection and radius of the membrane device. The formula for the radius of the spherical mirror (R) is

$$R = \frac{d^2 + r^2}{2d} \approx \frac{r^2}{2d} \text{ for } d \ll r, \quad (2-3)$$

where d is the deflection and r is the radius of the device in question.

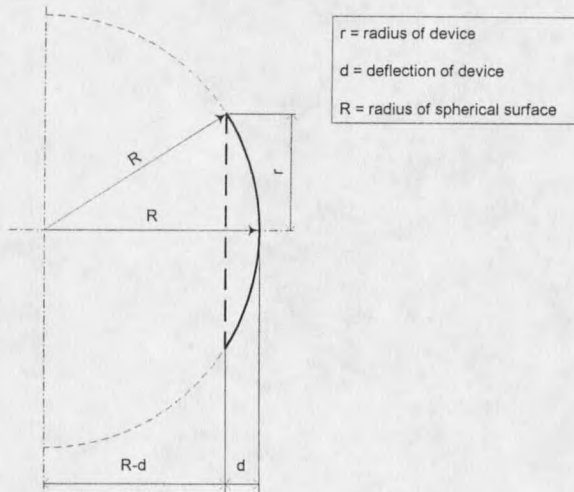


Figure 2-3. Radius of spherical reflector as function of device radius and deflection.

The resulting focal length as a function of center deflection of a device is shown in figure 2-4 for a $750\mu\text{m}$ and a $1500\mu\text{m}$ diameter device. Since the devices are assumed to be perfectly flat when no pressure is applied, the focal length of the membranes will be infinite at 0 deflection. The same amount of center deflection of devices of varying size will give different focal lengths. Assuming the same level of deflection for devices, the smaller the device is, the shorter its focal length will be. The focal length will change more rapidly with the initial deflection for a smaller device. This will result in a greater range of focus adjustment for small deflections of smaller devices.

